ORIGINAL PAPERS



Effects of photodeoxygenation on cell biology using dibenzothiophene S-oxide derivatives as O(³P)-precursors

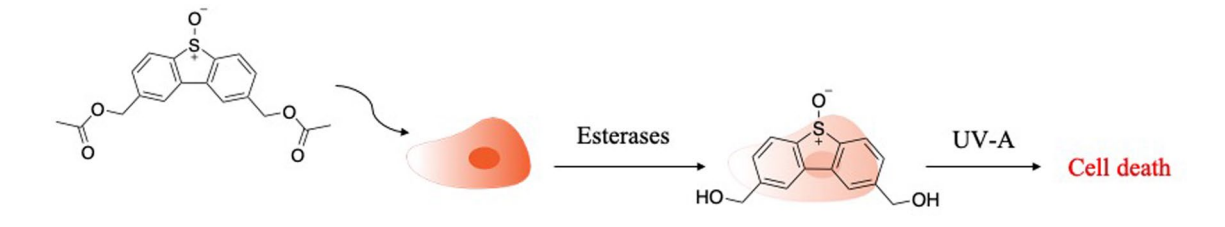
Ankita Isor¹ · Austin T. O'Dea¹ · Scott F. Grady¹ · John T. Petroff II¹ · Kristin N. Skubic¹ · Bashar Aziz¹ · Christopher K. Arnatt¹ · Ryan D. McCulla¹

Received: 23 August 2021 / Accepted: 8 November 2021 / Published online: 25 November 2021 © The Author(s), under exclusive licence to European Photochemistry Association, European Society for Photobiology 2021

Abstract

Photodeoxygenation of dibenzothiophene *S*-oxide and its derivatives have been used to generate atomic oxygen [O(³P)] to examine its effect on proteins, nucleic acids, and lipids. The unique reactivity and selectivity of O(³P) have shown distinct oxidation products and outcomes in biomolecules and cell-based studies. To understand the scope of its global impact on the cell, we treated MDA-MB-231 cells with 2,8-diacetoxymethyldibenzothiophene *S*-oxide and UV-A light to produce O(³P) without targeting a specific cell organelle. Cellular responses to O(³P)-release were analyzed using cell viability and cell cycle phase determination assays. Cell death was observed when cells were treated with higher concentrations of sulfoxides and UV-A light. However, significant differences in cell cycle phases due to UV-A irradiation of the sulfoxide were not observed. We further performed RNA-Seq analysis to study the underlying biological processes at play, and while UV-irradiation itself influenced gene expression, there were 9 upregulated and 8 downregulated genes that could be attributed to photodeoxygenation.

Graphical abstract



1 Introduction

Atomic oxygen $[O(^3P)]$ is an intriguing electrophilic oxidant that has high levels of reactivity with various functional groups; however, $O(^3P)$ also demonstrates notable selectivity when compared to other reactive oxygen species (ROS) like hydroxyl radical [1]. The study of $O(^3P)$ in the condensed phase was previously hindered by a lack of "clean" sources. This was primarily because of the harsh conditions required to generate the oxidant and the formation of by-products along with $O(^3P)$ [1, 2]. Opportunities for exploring the

Ryan D. McCulla ryan.mcculla@slu.edu

oxidative behavior of $O(^3P)$ in solution increased dramatically after $O(^3P)$ was determined to be a photodeoxygenation product of Dibenzothiophene *S*-oxide (DBTO) upon UV-A irradiation [3]. DBTO has since been used to study the reactivity profile of $O(^3P)$ and with a special focus on its selectivity for alkenes and thiols [4, 5].

The DBTO scaffold with its heterocyclic aromatic core is not ideal for studying the implications of O(³P) reactivity in biological conditions. The aromatic core contributes to poor water solubility and the need for UV-A irradiation increases the risk for off-target effects, particularly as exposure time increases, due to UV-sensitive groups in proteins and nucleic acids [6–8]. The risk of off-target effects can be mitigated by decreasing the time of UV irradiation to the point where there are no observable effects influencing the cells. DBTO



Department of Chemistry, Saint Louis University, 3501 Laclede Ave., St. Louis, MO 63103, USA

Fig. 1 A Photodeoxygenation of 1-SO releasing $O(^3P)$. B Hydrolysis of 1-SO by esterases to release 2-SO. Photodeoxygenation of 2-SO then releases $O(^3P)$ and 2-S (hydrolyzed form of 1-S)

has been derivatized to extend the chromophore [9, 10], and water-soluble substituents such as hydroxyl and sulfonic acid groups have been added to generate viable candidates for biological studies [11–13]. Photodeoxygenation of DBTO derivatives in aqueous media has strongly suggested O(³P) formation at acidic and neutral pH [11], which supports the feasibility of using DBTO derivatives as O(³P)-precursors in in-vitro studies. In the past decade, work exploring O(³P)-oxidation in proteins, nucleic acids, and lipids has been reported using DBTO derivatives [13-17]. These studies have illustrated O(³P)'s selectivity for thiols in the form of cysteine oxidation in proteins [13, 14], strand scission in pUC19 plasmid from O(³P) release [15], and unique lipid oxidation product profile that includes 2-hexadecenal, which has not been observed on oxidation with other ROS [17]. These results collectively map out the possibility of a cascade of events from O(³P) release in a global cellular environment.

In an attempt to evaluate the overall effect of O(³P) in a cell, we treated MDA-MB-231 cells with an aqueous-soluble DBTO derivative **1-SO** and studied the cellular response under different conditions. We hypothesized that **1-SO** would localize within cells and release O(³P) upon photodeoxygenation which would then trigger oxidative stress responses (Fig. 1A). The compound **1-SO** has been synthesized previously [11] and the expectation for cellular absorption of **1-SO** was based on the assumption that the ester groups flanking the DBTO core structure would cross the lipophilic cell membrane and hydrolyze to free hydroxyl

groups by esterases in the cell resulting in **2-SO** (Fig. 1B, hydrolyzed form of 1-SO) [18]. The subsequent O(³P) release from UV-A irradiation was then predicted to initiate cellular responses resulting in apoptosis as high levels of ROS are implicated in apoptotic signaling [19–22]. Accumulation of the compound in cells was confirmed using microscopy with the fluorescent sulfone derivative (1-SO₂) and the effects from O(³P)-release on cells were analyzed using cell viability and cell cycle phase determination assays. RNA-Seq analysis was performed to further examine the biological processes triggered by O(³P) release via 1-SO.

2 Results and discussion

2.1 Fluorescence microscopy using a sulfone derivative to observe cell permeability

Compounds **1-SO** and **1-S** were synthesized using methods described in the literature [11]. In an attempt to validate and observe these compounds' cell permeability, sulfone derivative **1-SO**₂ was synthesized as sulfone derivatives of DBTO have been shown to localize as fluorescent dyes in the nucleus, plasma membrane, and mitochondria [23–25]. The synthetic design to prepare **1-SO**₂ included a simple oxidation of **1-S** with *m*-Chloroperoxybenzoic acid overnight (Fig. 2A). Excitation and emission spectra for **1-SO**₂ in acetonitrile are shown in Fig. 2B, where an excitation scan was performed at 360 nm emission and emission scan



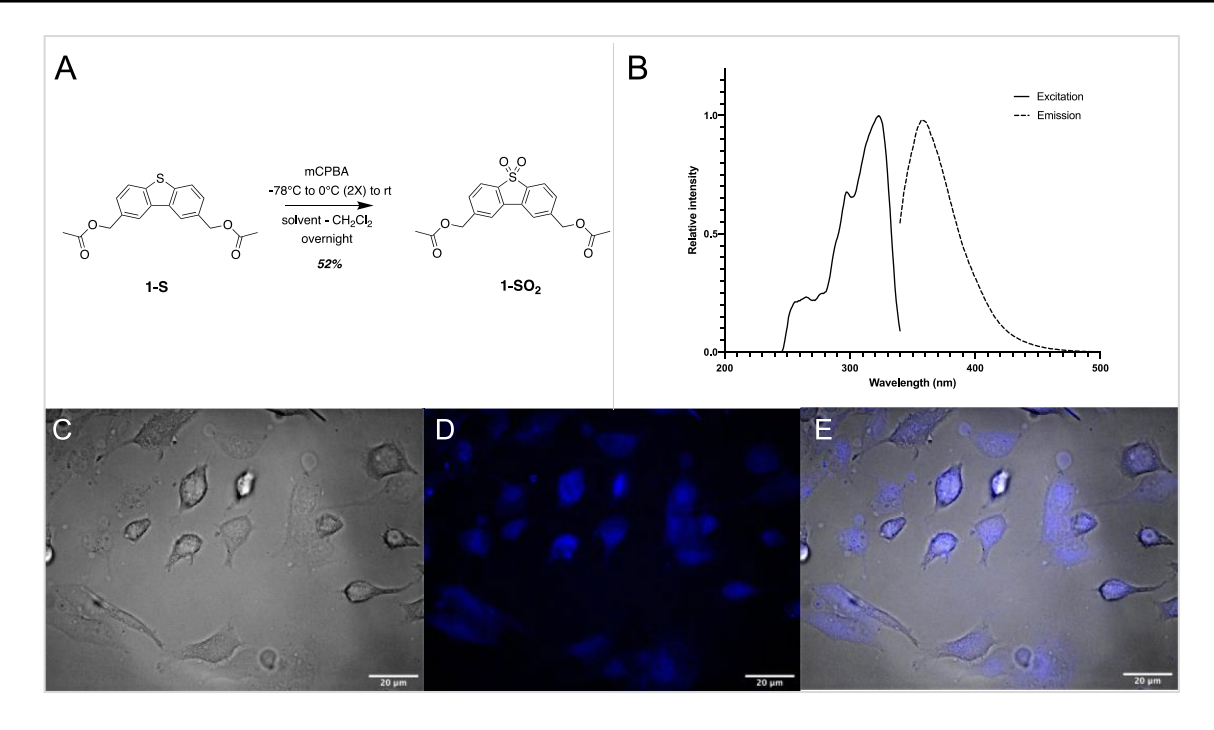


Fig. 2 A Synthesis of sulfone derivative 1-SO₂, B excitation and emission spectra for 1-SO₂ in CH₃CN, C brightfield image of cells stained with 1-SO₂, D fluorescence image (DAPI/UV filter set) of

cells stained with **1-SO₂** E merged composite image of C and D. Images annotated and processed using FIJI [26]

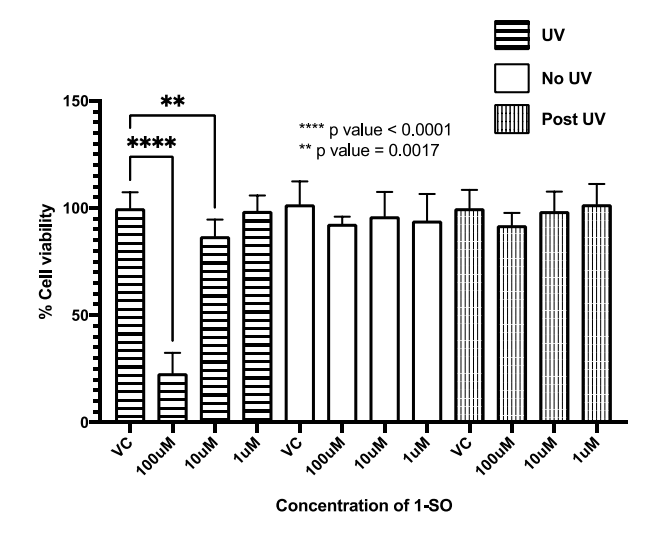
was performed by the exciting sample at 320 nm. The fluorescence excitation and emission spectra strongly suggested that **1-SO**₂ could be used to observe and predict the localization of **1-SO** within the cell. A DAPI/UV filter set to examine the cell uptake of **1-SO**₂ was used based on these measurements and poor absorption of **1-SO**₂ above 350 nm as noted in its UV–Visible spectra (SI, Section S1.3). Fixed cell imaging experiments were performed on HeLa cervical cancer cells as shown in Fig. 2C–E. Fluorescent derivative **1-SO**₂ was observed to diffuse within the cell uniformly with no specific localization observed in Fig. 2D and the composite image presented in Fig. 2E. These fluorescent microscopy images suggested that derivative **1-SO** can permeate the cell membrane and diffuse inside the cell indiscriminately.

2.2 Cell viability assays as a function of concentration and time

The next step was to assess the cell viability of **1-SO** in a concentration and time-dependent manner in MDA-MB-231 cells. Cell viability assay was designed to include three experimental conditions based on UV-exposure: (a) UV—where cells were introduced to compounds and then irradiated with UV-A light, (b) **No-UV**—where cells were introduced to compounds and not irradiated with UV-A light, and (c) **Post-UV**—where cells were irradiated with UV-A light before introducing them to the compounds. Different time points of 15 min, 30 min, and one hour

were tested with various concentrations of **1-SO** (100 μ M - 1 nM) to select a reasonable duration for UV exposure (SI, Section S2.1). The results for 15 min irradiation showed a slight decrease in cell viability for 100 µM **1-SO** for **UV** condition [80.3%, p value 0.0049 compared to Vehicle Control (VC), post-hoc ANOVA] with no decrease observed for 100 µM 1-SO in No-UV and **Post-UV** condition. The results from 30 min irradiation showed a significant decrease in cell viability for 100 µM **1-SO** in **UV** condition (18.9%, p-value < 0.0001 compared to VC, post-hoc ANOVA) with no such observable effect for 1-SO in No-UV and Post-UV conditions. In one-hour irradiation experiments, complete cell death was observed for 100 μ M **1-SO** in **UV** (-8.44%, p value < 0.0001 compared to VC, post-hoc ANOVA) with no decrease in cell viability detected in No-UV and Post-UV conditions for 100 μM **1-SO**. Based on these results, we designed followup experiments with a 30 min irradiation time as 15 min of UV-A irradiation decreased cell viability by only modest amounts and one hour of UV-A irradiation resulted in complete cell death for 100 µM 1-SO. Raw absorbances for VC were plotted as a function of time to determine differences in cell viability to examine the effect of UV-A irradiation alone on cell survival for MDA-MB-231 cells (SI, S2.2, Fig. S4). The raw absorbance values were not drastically different across time points and the various treatment conditions suggested that UV-A exposure did not cause a significant decrease in cell viability by itself.





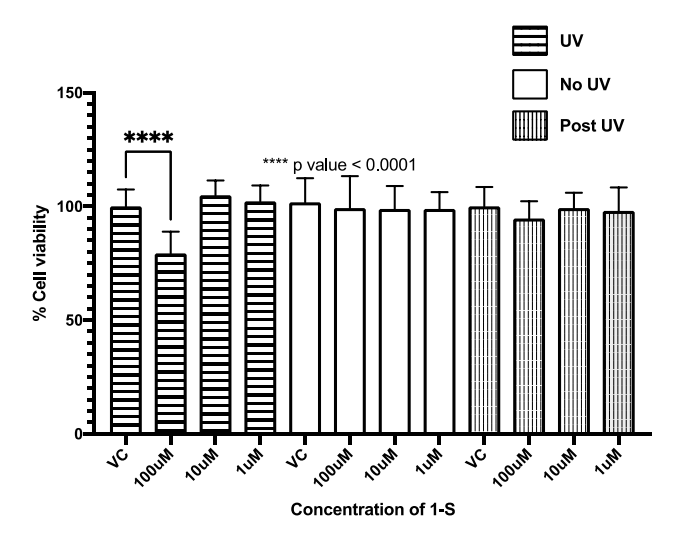


Fig. 3 MTS assay cell viability results for **1-SO** and **1-S** after 30 min of UV-A irradiation (VC – Vehicle Control, n=6, plot—mean with SD, post-hoc one-way ANOVA analysis with Tukey's test) (Data for Vehicle Control (VC) has been presented in ref [25])

As photodeoxygenation of **1-SO** involves two photoproducts, $O(^3P)$ and corresponding sulfide **1-S**, sulfide **1-S** was included in the assays and analyses for all experimental conditions to serve as a control. This approach was undertaken to compare the results of compound **1-S** to the results of **1-SO** in **UV** to determine the sole biological effect of $O(^3P)$ -oxidation. Figure 3 presents the results for cell viability with **1-SO** and **1-S** examined at 30 min UV-irradiation. No significant decrease in cell viability was observed for **1-S** in **UV**, **No-UV**, and **Post-UV** setups except for 100 μ M in **UV** (79.33 \pm 9.57%, Mean \pm STDEV), which indicated that **1-S** is not intrinsically cytotoxic. This finding by extension strongly implied that any drastic decrease in cell viability observed for **1-SO** in **UV** is likely a result of $O(^3P)$ release. Cell viabilities decrease to $23.02 \pm 9.43\%$ and $86.91 \pm 7.75\%$



100 μM of Compound	Concentration of corresponding sulfide (µM)
1-SO $(n=8)$	5.2±0.3
Hydrolyzed form– 2-SO $(n=4)$	25.5 ± 4.3

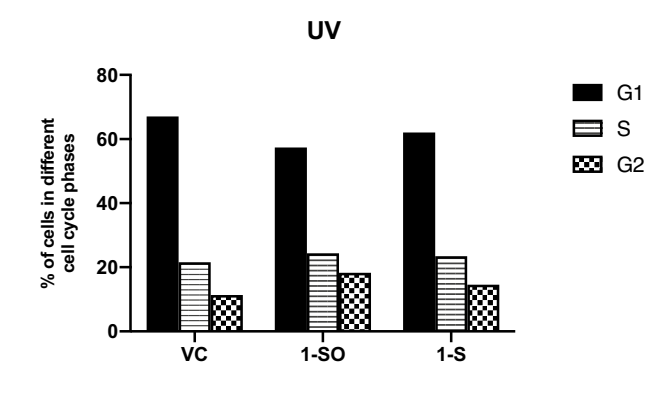
with **1-SO** treatment in **UV** was observed at 100 μ M and 10 μ M, respectively. This decrease in cell viability for **1-SO** in **UV** was substantial when compared to **1-S** and indicated that cell death was reasonably caused by photodeoxygenation reaction as **1-SO** and **1-S** weren't found to be cytotoxic without irradiation (**No-UV**). Cell viability assay results for lower concentrations of **1-SO** and **1-S** are included in Fig. S5 in SI.

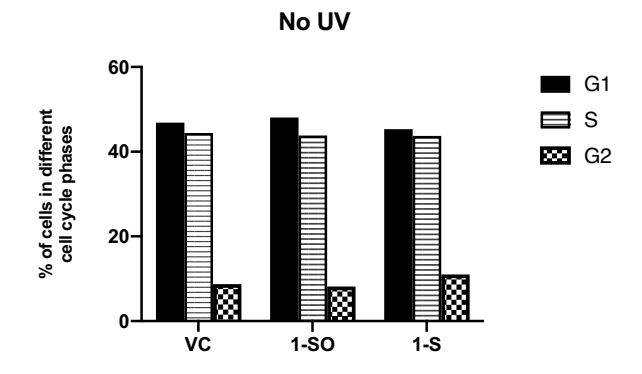
2.3 Photodeoxygenation experiment in media to estimate the extent of O(³P) formation and cell cycle phase determination assay

Photodeoxygenation experiments in media without cells were performed at 100 µM concentrations of 1-SO and 2-SO (hydrolyzed form of 1-SO). This experiment was aimed at estimating the extent of S–O cleavage in in-vitro studies. The treatment conditions described as UV, No-UV, and Post-UV were replicated for 30 min. The results are summarized in Table 1, which demonstrate that close to 5–25% of 1-SO or its hydrolyzed form 2-SO was likely photodeoxygenating under the treatment conditions for the above-described cell viability assays. No sulfide generation was observed in No-UV and Post-UV setups. This extent of photodeoxygenation is indicative of potentially low to moderate levels of O(³P) generated on S-O cleavage of 1-SO or its hydrolyzed form **2-SO**. The significant decrease in cell viability observed for 10 μM **1-SO** in UV is notable for such low-to-moderate levels of photodeoxygenation.

Cell cycle phase determination assay was performed for **1-SO** and **1-S** at 10 μ M in UV, No-UV, and Post-UV conditions (Fig. 4). The data did not show any significant differences between the distribution of cells in each phase for VC, **1-SO**, and **1-S** within individual treatment conditions. However, differences were observed when treatment conditions were compared to each other. The cell distribution profiles were similar for UV and Post-UV but were significantly different when compared to No-UV for both **1-SO**, **1-S**, and VC. This was possibly due to UV irradiation involved in UV and Post-UV treatment where $\sim 60-70\%$ and $\sim 20-25\%$ of cells were in G1 and S phases whereas $\sim 45\%$ of cells were in each both G1 and S phases for No-UV condition. This supports the general understanding of UV light having an effect on the cell cycle and possibly delaying cell division







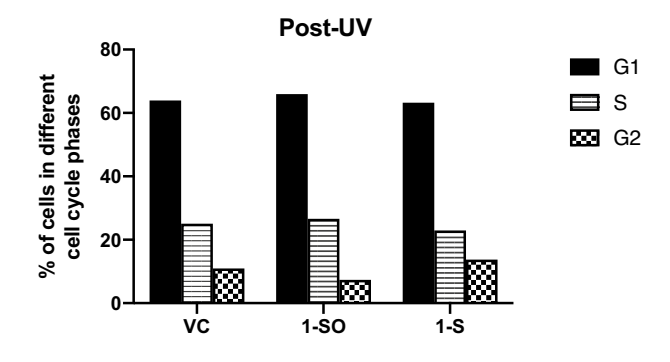


Fig. 4 Cell cycle phase determination assay (*VC* vehicle control) for **1-SO** and **1-S** after 30 min of UV-A irradiation post-addition of 1-SO (UV), no UV-A treatment after addition of compounds (**No-UV**), and addition of compounds post-UV-A irradiation (**Post-UV**) (Data for Vehicle Control (VC) has been presented in ref [25])

[27], as a lower proportion of cells was observed in the S phase for UV-associated conditions in MDA-MB-231 cells, as compared to **No-UV** condition.

2.4 RNA-sequencing analysis

To further investigate the observed decrease in cell viability for **1-SO** in **UV**, we performed an RNA-seq analysis for two treatment conditions **UV** and **No-UV**. This was a preliminary study to observe affected cellular mechanisms

and generate hypotheses for future studies. Examination of the transcriptome followed by differentially expressed gene (DEG) and pathway analyses was used to draw insights into the effects of photodeoxygenation on cell pathways and biological processes. The data set for VC in UV and No UV where cells were suspended in 1% DMSO in DMEM has been presented previously in a report ("sister study") where the RNA-seq analyses for compounds profiled in the report were performed in conjunction with the experiments outlined here [25]. Figure 5 shows a heatmap outlining the cluster analysis of genes across different treatment conditions for 1-SO and VC (1% DMSO in DMEM). The heatmap compares gene expression across UV and No UV treatment conditions for 10 µM 1-SO and VC where red indicates genes with higher FPKM counts and blue shows genes with lower FPKM counts. The color gradient is scaled across the row so expression levels can be compared for similar and related genes across treatment conditions. The cluster analysis implies that the gene expression profile of 1-SO_No UV is similar to VC_No UV and 1-SO_UV resembles VC_UV. This reflects the observations from the cell cycle phase study where VC UV and 1-SO UV cell distribution were similar to each other but notably different from VC_No UV and 1-SO_NoUV.

To study the DEG list for these treatment conditions with 1-SO and VC, we used the threshold values for p < 0.005 and $\log_2(\text{fold change}) < -1.5$ for downregulated genes and $\log_2(\text{fold change}) > 1.5$ for upregulated genes (SI, Section S3.1). On comparing VC_UV and VC_No UV using these parameters, we found 25 upregulated genes and 38 downregulated genes. These findings suggested that UV influenced gene expression as observed in Fig. 5. The DEG analysis for VC_UV and VC_No UV was performed in the "sister study" using different parameters ($p_{\text{adj}} < 0.05$, $\log_2(\text{fold change}) < -1$ and > 1 for downregulated and upregulated) where 3 upregulated and 5 downregulated genes were discussed in detail to highlight the effect of UV exposure on MDA-MB-231 cells [25].

We then focused on comparing **1-SO_UV** to **VC_UV** and **1-SO_No UV** to **VC_No UV** to understand the effect of O(³P)-release. The volcano plots presenting DEG analysis for **1-SO_UV v. VC_UV** and **1-SO_No UV v. VC_No UV** are included in Fig. 6A–B. There were 9 upregulated and 8 downregulated genes observed for **1-SO_UV v. VC_UV**. Among these upregulated and downregulated genes, some of the notable ones are highlighted in Fig. 6A. We observed overexpression of *IGFBP2* which is involved in IGFBP2/IGF1/IGF1R pathway engaging in cancer-related endothelial recruitment (OMIM: 146731) [30, 31]. We also observed overexpression of *LIN28A* (OMIM: 611403) and *ARHGAP9* (OMIM: 610576) [30]. *LIN28A* is an important gene for skeletal muscle differentiation and targets IGF2, which is crucial for muscle tissue growth and differentiation [32].



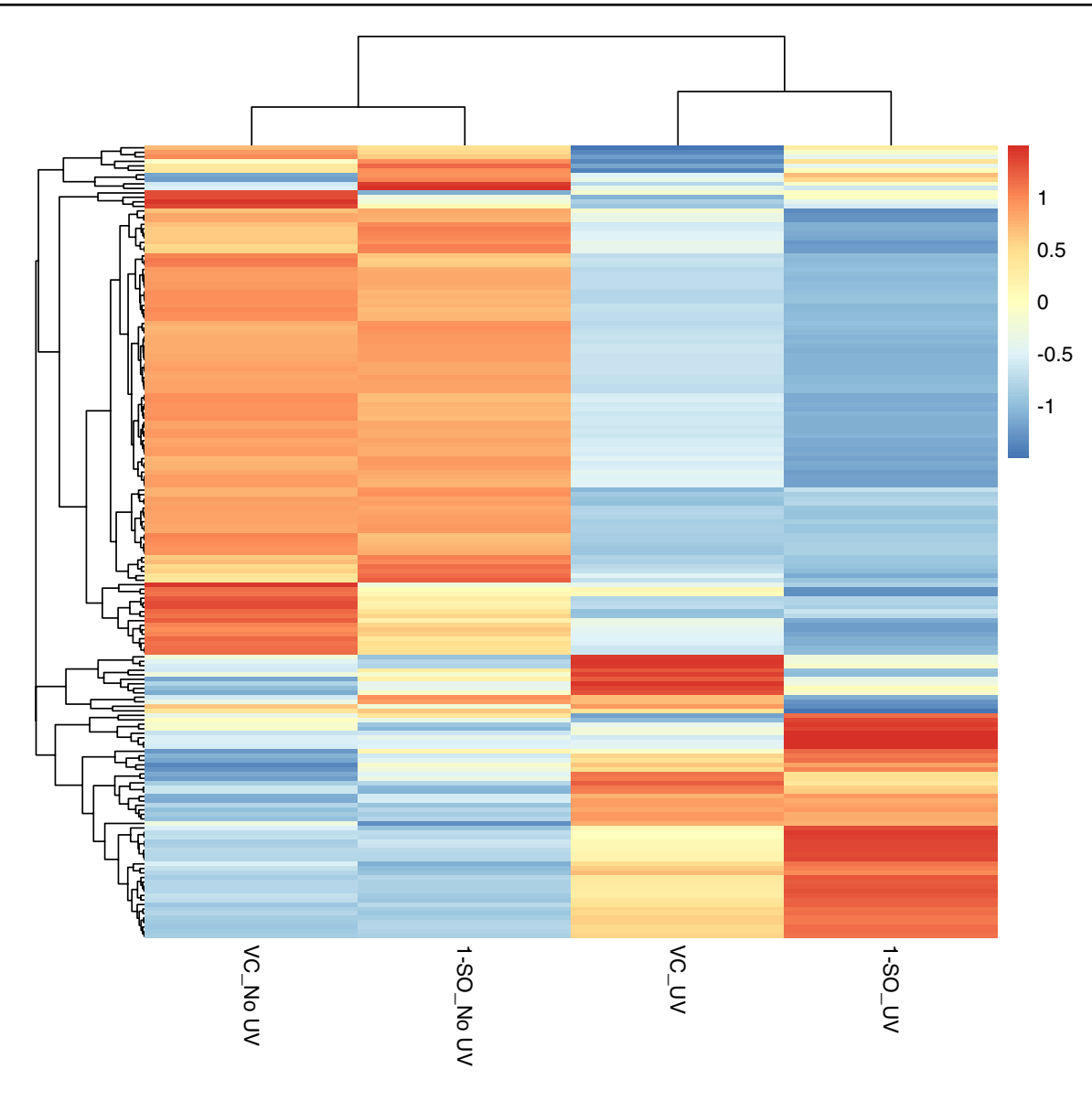


Fig. 5 Heatmap for cluster analysis of differentially expressed genes for 1-SO in different treatment conditions compared to VC (n=1, Red-higher FPKM read counts, Blue-lower FPKM read counts, gen-

erated using R pheatmap package) [28, 29]. (Data for VC_UV and VC_No UV have been presented in ref [25])

Interestingly, LIN28A is also one of the four genes that are "sufficient to reprogram human somatic cells to pluripotent stem cells that exhibit the essential characteristics of embryonic stem cells" [33]. ARHGAP9 is implied in regulating cell migration and adhesion with recombinant ARHGAP9 shown to have considerable GAP activity towards RAC1 and CDC42 [34, 35]. Among the downregulated genes, we observed an under-expression of GABRA3 (OMIM: 305660), RALGPS1 (OMIM: 614444), NCAM2 (OMIM: 602040) [30]. We similarly evaluated 1-SO_No UV v. VC_No UV and found 8 upregulated and 3 downregulated genes. A similar analysis was performed for 1-S in UV and 1-S in No UV where gene expression was evaluated across treatment conditions using a heatmap (SI, Section S3.2, Figure S6). The

differentially expressed genes of **1-SO_UV v. VC_UV** were compared to **1-S_UV v. VC_UV** to eliminate effects from resulting sulfide upon photodeoxygenation, but no common set of genes was found between the two samples (SI, Section S3.3, Figure S7). Overall, the low number of genes annotated in the DEG analysis and corresponding heatmap strongly suggest that photodeoxygenation (**1-SO_UV**) initiated by UV when compared to **VC_UV** by itself has a modest or negligible effect on gene expression; on the other hand, the effect of UV exposure alone is more pronounced than the effect of the treatment with **1-SO** in UV.

We finished our examination of diffusing O(³P)'s effect on cell biology by performing pathway analysis using genes annotated as upregulated and downregulated for **1-SO_UV**



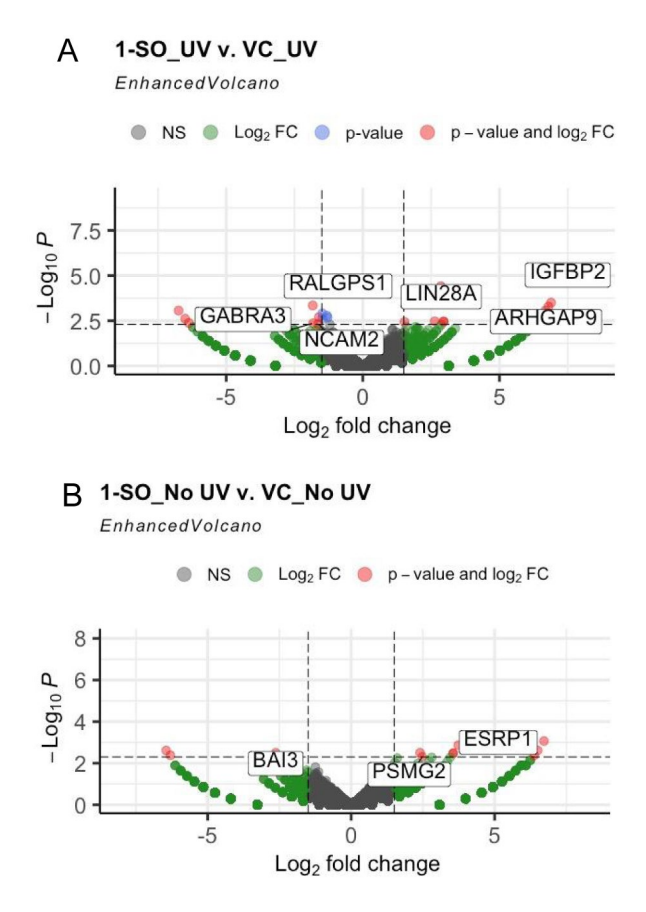


Fig. 6 A Volcano plot outlining DEG analysis of 1-SO_UV v. VC_UV generated using Enhanced Volcano package from Bioconductor in R $(n=1, p \text{ value} < 0.005, \text{ upregulated } \log_2(\text{fold change}) > 1.5, \text{ downregulated } \log_2(\text{fold change}) < -1.5). [28, 36, 37].$ **B** $Volcano plot outlining DEG analysis of 1-SO_No UV v. VC_No UV generated using Enhanced Volcano package from Bioconductor in R <math>(n=1, p \text{ value} < 0.005, \text{ upregulated } \log_2(\text{fold change}) > 1.5, \text{ downregulated } \log_2(\text{fold change}) < -1.5) [28, 36, 37] (Data for VC_UV and VC_No UV have been presented in ref [25])$

v. VC_UV DEG analysis through the ToppGene suite of programs (SI, Section S3.1, Table S1) [38–40]. The pathway analysis did not yield terms related to ROS metabolic processes or oxidative stress. This was expected because the genes/gene products identified from DEG analysis of 1-SO_UV v. VC_UV are not typically implicated in maintaining ROS homeostasis or response to oxidative stress [41, 42]. The pathway analysis for the upregulated and downregulated genes as a function of -log₁₀ (p-value) are presented in Fig. 7. The pathways annotated in Fig. 7 are consistent with the genes discussed above. According to the pathway analysis of upregulated genes, *IGFBP2* was involved in insulinlike growth factor signaling, ghrelin, photodynamic therapyinduced HIF-1 survival signaling, *ARHGAP9* was annotated in the regulation of RAC1 and RhoA activities, and *LIN28A*

is implied in cardiac progenitor differentiation. The pathway analysis for downregulated genes outlined cardiac protection against ROS, gamma-aminobutyric acid receptor life cycle, GABA receptor signaling, mBDNF, and proBDNF regulation of GABA neurotransmission, and rett syndrome causing genes from *GABRA3*. Within the same analysis, *NCAM2* was marked for prion diseases and cell adhesion molecules.

3 Conclusion

In conclusion, we observed a significant decrease in cell viability from photodeoxygenation of 1-SO in MDA-MB-231 cells at 100 µM. Since cell viability decrease wasn't observed for 1-S or 1-SO without irradiation (No-UV) in different treatment conditions, it can be reasonably concluded that the observed decrease in cell viability can be attributed to photodeoxygenation. Cell cycle phase determination assay did not reveal any significant difference between cell distribution across different phases between VC, 1-SO, and 1-S within each treatment condition. Preliminary RNA-seg analysis revealed that photodeoxygenation of 1-SO did not have a remarkable effect on gene expression. This was most likely due to the low extent of photodeoxygenation (5-25%) that led to only small amounts of O(⁵P) generation. It is interesting to note that the minuscule amounts were significant to result in cell death but were probably not significant enough to influence gene expression. Pathway analyses did not indicate any terms common with annotations included in ROS metabolic processes and oxidative stress. The findings from this study illustrate an interesting environment within the cell that needs further examination to uncover the underlying mechanisms behind the observed decrease in cell viability. These studies can be designed to include different cell lines, higher irradiation times to increase O(³P) generation, higher sample sizes for RNA-seq supplemented by qRT-PCR, and eventually conducting in-vivo studies to confirm the findings.

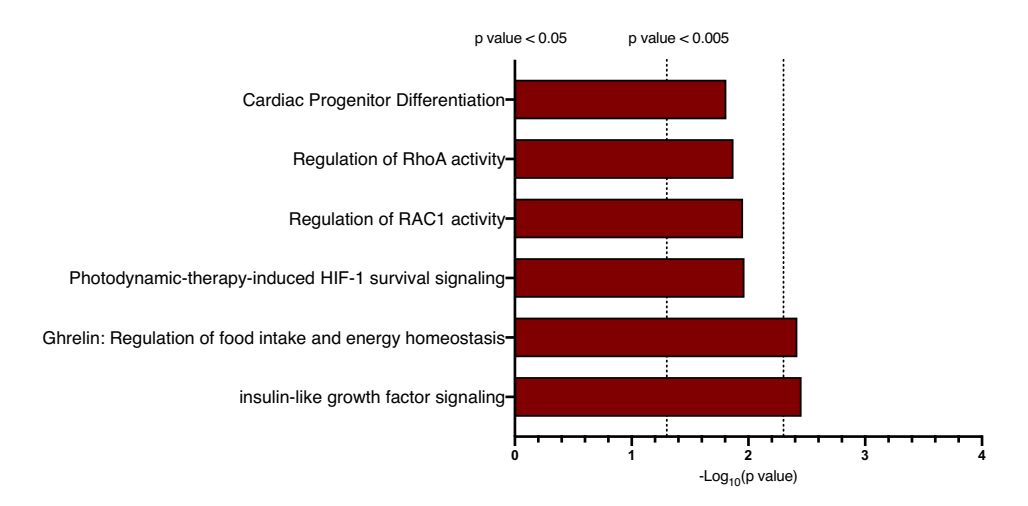
4 Experimental

All solvents and reagents were bought from Fisher Scientific or Millipore Sigma. All buffers and cell media were purchased from Sigma Aldrich. ACS grade solvents were used for synthetic procedures and NMR solvents were acquired from Cambridge Isotope Laboratories or Millipore Sigma. Compounds were characterized using Gas Chromatography-Mass Spectrometry (GCMS), UV–Visible spectroscopy, NMR spectroscopy, and High-Res Mass Spectrometry (HRMS) methods. GCMS was performed on Shimadzu GCMS-QP2010S, UV–Visible spectroscopy was performed on Thermo Fisher Scientific

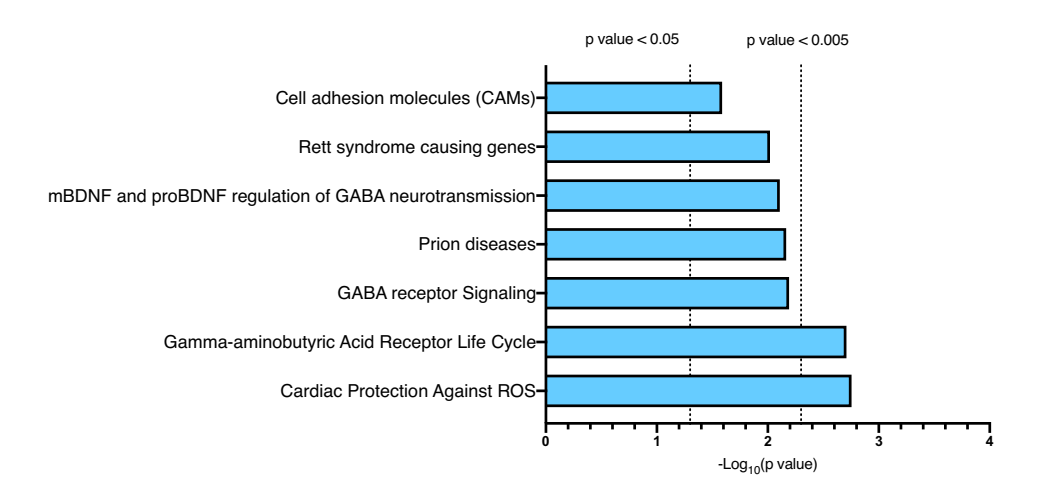


Fig. 7 Significant terms from pathway analysis of A upregulated genes and B downregulated genes identified in 1-SO_UV v. VC_UV

A. Significant terms for Pathway analysis: upregulated genes



B. Significant terms for Pathway analysis: downregulated genes



Nanodrop 2000c, NMR spectra were obtained on Bruker NMR 400 MHz Avance III, and HRMS was performed on Orbitrap Q-Exactive (Thermo Fisher Scientific). Highperformance flash chromatography for purification was performed on a Biotage system with a Biotage Horizon detector or CombiFlash NextGen 100 (Teledyne ISCO). High-Pressure Liquid Chromatography (HPLC) analyses were performed on Agilent 1200 series (Quad pump, DAD, autosampler). The column (5 µm, 150 X 4.6 mm, C-18) used on HPLC was acquired from Higgins Analytical. Fluorescence spectra for 1-SO₂ were acquired on Shimadzu Fluorometer RF-5301 PC. Photodeoxygenation experiments were carried out on a Luzchem photoreactor with 8 LZC-UVA bulbs (Hitachi FL8BL-B, fwhm: 325-375 nm). All statistical analyses were performed on GraphPad Prism and Microsoft Excel. Graphs were generated using GraphPad Prism and R [28].

4.1 Detailed synthetic procedures

4.1.1 Synthesis of dibenzothiophene and dibenzothiophene S-oxide derivatives

Compounds **1-S** (2,8-diacetoxymethyldibenzothiophene), **1-SO** (2,8-diacetoxymethyldibenzothiophene *S*-oxide), hydrolyzed form **2-S** (2,8-dihydroxymethyldibenzothiophene), and hydrolyzed form **2-SO** (2,8-dihydroxymethyldibenzothiophene *S*-oxide) were synthesized using methods described in Korang et al., 2010 [11].



4.1.2 Spectral results

for 2,8-diacetoxymethyldibenzothiophene (1-S)

¹H-NMR (400 MHz, CDCl₃): δ 8.18 (s, 2H), 7.86 (d, J=8.2 Hz, 2H), 7.49 (d, J=8.2 Hz, 2H), 5.30 (s, 4H), 2.14 (s, 6H).

Spectral results are consistent with previously published results in literature [11].

GCMS (EI): *m/z* (%): 226.05 (85.65%), 269.10 (100%), 328.05 (93.73%). Calcd MW: 328.38.

4.1.3 Spectral results

for 2,8-diacetoxymethyldibenzothiophene-S-oxide (1-SO)

¹H-NMR (400 MHz, CDCl₃): δ 8.00 (d, J = 7.8 Hz, 2H), 7.83 (s, 2H), 7.52 (d, J = 8.3 Hz, 2H), 5.23 (s, 4H), 2.17 (s, 6H).

Spectral results are consistent with previously published results in literature [11].

HRMS (ESI+): calcd. [M+H] 345.0791, observed 345.0785.

4.1.4 Spectral results

for 2,8-dihydroxymethyldibenzothiophene (2-S, hydrolyzed form of 1-S)

¹H-NMR (400 MHz, DMSO-d₆): δ 8.25 (s, 2H), 7.95 (d, 2H, J=8.2 Hz), 7.47 (dd, 2H, J=8.0 Hz, 1.1 Hz), 5.33 (t, 2H, J=5.7 Hz), 4.68 (d, 4H, J=5.8 Hz).

Spectral results are consistent with previously published results in literature [11].

GCMS (EI): *m/z* (%): 185.05 (100%), 227.05 (27.56%), 244.10 (80.92%). Calcd MW: 244.31.

4.1.5 Spectral results

for 2,8-dihydroxymethyldibenzothiophene S-oxide (hydrolyzed form of 1-SO)

¹H-NMR (400 MHz, DMSO-d₆): δ 8.01 (d, 4H, J= 8.2 Hz), 7.52 (d, 2H, J= 7.8 Hz), 5.48 (t, 2H, J= 5.7 Hz), 4.65 (d, 4H, J= 5.7 Hz).

Spectral results are consistent with previously published results in literature [11].

HRMS (ESI+): calcd. [M+H] 261.0580, observed 261.0576.

4.1.6 Synthesis of 1-SO₂

1-S (150.4 mg, 0.4584 mmol) was dissolved in 20 mL CH₂Cl₂ and added to a 50 mL round bottom flask with a stir bar on a dry-ice acetone bath. Oxidizing agent, *m*-Chloroperoxybenzoic acid (77% w/w, 206.8 mg, 0.9227 mmol),

was dissolved in 15 mL CH₂Cl₂ and added to an additional funnel which was fixed onto the round bottom flask under nitrogen atmosphere. The oxidizing agent was slowly added using the addition funnel over one hour while stirring. The addition funnel was then removed from the setup. The temperature of the bath was allowed to reach 0 °C and dry ice was then added to decrease the temperature. This process of temperature cycling was continued for one more cycle. The temperature was then allowed to increase overnight. The reaction solution was then washed using a saturated solution of NaHCO₃ once and Millipore water four times. The organic layer was then dried using anhydrous MgSO₄. The solvent was removed under reduced pressure and purified using high-pressure flash chromatography (70% EtOAc: 30% Hexanes, R_f =0.75). The purification yielded 85.8 mg (52.0%) of a white powdery solid.

¹H-NMR (400 MHz, CDCl₃): δ 7.84 (s, 1H), 7.82 (d, J=4.2 Hz, 3H), 7.54 (d, J=7.9 Hz, 2H), 5.22 (s, 4H), 2.18 (s, 6H).

¹³C-NMR (100 MHz, CDCl₃): δ 170.79, 142.79, 137.95, 132.01, 130.35, 122.73, 121.39, 65.35, 21.15.

HRMS (nanoESI+): m/z [M+H]⁺ calculated for $[C_{18}H_{17}O_6S]^+$ 361.0740, observed m/z 361.0737.

4.2 Fluorescence imaging

Coverslips (NeuVitro, poly-D-lysine-coated #1.5 thickness) were pre-incubated with culture medium and placed into the wells of a six-well plate. HeLa cells were cultured using RPMI media supplemented with 10% FBS and 1% penicillin-streptomycin. A cell suspension with a density of 5.5×10^5 cells mL⁻¹ was prepared and added in volumes of 2 mL onto a six-well plate with coverslips. The six-well plate was then placed in an incubator at 37 °C, 5% CO₂ overnight. After the incubation, the plates were aspirated, and then a solution DPBS of $1-SO_2$ (1.8 mL DPBS + 200 μL of 50 μM stock in 1% DMSO in PBS, final concentration $-5 \mu M$) was pipetted onto the cell monolayers adhering to the coverslips. The cells on the coverslip were allowed to incubate for 15 min post-compound addition. The cells were then washed using DPBS and subsequently treated with 4% of paraformaldehyde solution prepared in DPBS and then incubated at room temperature for 30 min to ensure full fixation. Three washes of the coverslips with 1 mL DPBS were performed to rinse off any excess solution. The coverslips were then removed and mounted on slides with Thermo Fisher Scientific ProLong Gold Antifade Mountant. The samples were then dried for several minutes and sealed with a clear nail enamel before fluorescence microscopy.

Fluorescence microscopy for imaging was performed on Leica DM 4000B microscope and images were captured on a DFC3000G camera (Leica Microsystems-Germany) with 40X lens or 63X oil immersion. Leica LASX Core software



was used to acquire the images and 1-SO₂ was visualized using DAPI/UV-filter set. All images were processed on FIJI [26].

4.3 Cell studies

Please note that cell studies were performed alongside work reported in Ref [25]. Footnotes have been used in the SI to refer to data that has been presented in Ref [25].

4.3.1 Cell culture

MDA-MB-231 cell line was bought from ATCC (Manassas, VA). The cells were cultured in DMEM media supplemented with 10% FBS, 1% L-Glutamine, and 1% penicillin–streptomycin. The cells were incubated in 95% relative humidity with 5% CO_2 at 37 °C.

4.3.2 Cell viability assay

MDA-MB-231 cells were plated at 10,000 cells/well on three 96-well clear plates labeled as UV, No-UV, and Post-UV. All three plates were then incubated for 24 h. Varying concentrations of 1-SO and 1-S were added to two plates marked as UV and No-UV and all three plates were incubated for 15 min to one-hour post-compound addition. Plates UV and Post-UV were then placed in a Luzchem photoreactor with 8 LZC-UVA (Hitachi FL8BLB) bulbs for 30 min. The No-UV plate was placed next to the photoreactor covered in aluminum foil to serve as control during these 30 min. After UV exposure, compound solutions were added to the Post-UV plate and all three plates were then incubated for 24 h overnight. Cell antiproliferation assay using MTS-PMS reagent was performed based on the protocol described in the literature [43]. Flexstation3 multimode plate reader was used to record absorbance and data processing and analysis were performed on GraphPad Prism.

4.3.3 Photodeoxygenation studies

A 300 μ M stock solution in 1% DMSO in PBS of **1-SO** was prepared. In three 96-well plates, 100 μ L of DMEM solution was pipetted onto wells and in two plates (UV and No-UV) 50 μ L of stock solution was added to DMEM solution to reach a final 100 μ M concentration of **1-SO**. All three plates were incubated from 15 min – one hour and then the plates UV and Post-UV were irradiated for 30 min in a Luzchem photoreactor with 8 LZC-UVA bulbs. No-UV plate was kept in the dark for those 30 min. After UV-A exposure, the plates were incubated overnight. Corresponding sulfide **1-S** formation was monitored by diluting 100 μ L of the samples from the well with 400 μ L of acetonitrile and analyzing the

samples in HPLC. The same procedure was used to evaluate photodeoxygenation of 2-SO (hydrolyzed form).

4.3.4 Cell cycle phase determination assay

MDA-MB-231 cells were seeded in three 6-well plates (UV, No-UV, and Post-UV) with a cell density of 1×10^6 cells/2 mL/well. Compounds 1-SO and 1-S were added to the wells at 10 µM final concentration to the plates labeled UV and No-UV. The plates were then incubated for 30 min and then plates marked UV and Post-UV were irradiated in the photoreactor with 8 LZC-UVA bulbs for 30 min and No-UV plate served as photocontrol (wrapped with aluminum foil and placed next to the photoreactor). Compounds 1-SO and 1-S were added to the Post-UV plate after photo-irradiation and all three plates were then incubated overnight. The cell cycle phase was analyzed through Cell Cycle Phase Determination Kit (Cayman Chemical, Ann Arbor, MI). Adherent cells were then washed in PBS and fixed in 200 μ L 1 × fixation buffer. The cells were then incubated at 4–8 °C for at least two hours in the dark. A 500 μL solution of PI DNA staining was added for another 30 min at room temperature in the dark. Flow cytometry analysis was then performed to determine the cell cycle phase.

4.3.5 RNA-Seq and transcriptome analysis

MDA-MB-231 cells were plated on two 6-well plates $(6 \times 10^5 \text{ cells/1.8 mL/well})$ marked UV and No-UV. Compounds 1-SO and 1-S were added at a final concentration of $10 \,\mu\text{M}$ (VC–1% DMSO) and the plates were then incubated. The UV plate was further exposed to UV-A irradiation in a photoreactor for 30 min post-incubation. After UV exposure, a total RNA purification kit (Sigma Aldrich, Catalog #RNB100) was used to extract RNA from these samples (n=1) for compound in each treatment condition). Sequencing and bioinformatics analysis were performed by Novogene Corporation. The raw data and processed files used for cluster and differential expression of gene (DEG) analyses are accessible through Geo (NCBI-Gene Expression Omnibus) [44, 45] series accession number GSE176382¹. Heatmaps and volcano plots were generated using pheatmap and Enhanced Volcano v1.8.0 (in Bioconductor) [37, 46] packages in R [28, 29, 36]. Union for cluster spreadsheet was filtered to generate heatmap in the appendix to exclude genes that had n = 1 or less across the four treatment conditions for z-score calculation through pheatmap package.

Pathway analyses were performed using the ToppGene suite of programs [38–40]. The DEG list comparing gene expression between treatment conditions was filtered for



Data for VC_UV and VC_No UV have been presented in ref [25]

p < 0.005 and $\log_2(\text{fold change}) < -1.5$ for downregulated and > 1.5 for upregulated genes. The HGNC symbols of the genes were then input as training gene sets to generate pathway terms from KEGG [47–49], BioCarta [50], BioCyc [51], Reactome [52–57], GenMAPP [58], MSigDB [59–61], and Pathway Ontology [62].

Supplementary Information The online version contains supplementary material available at https://doi.org/10.1007/s43630-021-00136-5.

Acknowledgements This work was supported by the National Science Foundation CHE-1900417.

Declarations

Conflict of interest There are no conflicts to declare.

References

- Bucher, G., & Scaiano, J. C. (1994). Laser flash photolysis of pyridine N-Oxide: Kinetic studies of atomic oxygen [O(3P)] in solution. *Journal of Physical Chemistry*, 98(1), 12411–12413.
- Lucien, E., & Greer, A. (2001). Electrophilic oxidant produced in the photodeoxygenation of 1,2-benzodiphenylene sulfoxide. *Journal of Organic Chemistry*, 66(13), 4576–4579. https://doi. org/10.1021/jo010009z
- Gregory, D. D., Wan, Z., & Jenks, W. S. (1997). Photodeoxygenation of dibenzothiophene sulfoxide: Evidence for a unimolecular S-O cleavage mechanism. *Journal of the American Chemical Society*, 119(1), 94–102. https://doi.org/10.1021/ja962975i
- Thomas, K. B., & Greer, A. (2003). Gauging the significance of atomic oxygen [O(3P] in sulfoxide photochemistry. A method for hydrocarbon oxidation. *Journal of Organic Chemistry*, 68(5), 1886–1891. https://doi.org/10.1021/jo0266487
- Omlid, S. M., Zhang, M., Isor, A., & McCulla, R. D. (2017). Thiol reactivity toward atomic oxygen generated during the photodeoxygenation of dibenzothiophene S-oxide. *Journal of Organic Chemistry*, 82(24), 13333–13341. https://doi.org/10.1021/acs.joc.7b02428
- Rastogi, R. P., Richa, K., Kumar, A., Tyagi, M. B., & Sinha, R. P. (2010). Molecular mechanisms of ultraviolet radiation-induced DNA damage and repair. *Journal of Nucleic Acids*, 2010, 592980. https://doi.org/10.4061/2010/592980
- Pattison, D. I., Rahmanto, A. S., & Davies, M. J. (2012). Photooxidation of proteins. *Photochemical and Photobiological Sciences*, 11, 38–53. https://doi.org/10.1039/c1pp05164d
- Roy, S. (2017). Impact of UV radiation on genome stability and human health. Advances in Experimental Medicine and Biology, 996, 207–219. https://doi.org/10.1007/978-3-319-56017-5_17
- Zheng, X., Baumann, S. M., Chintala, S. M., Galloway, K. D., Slaughter, J. B., & McCulla, R. D. (2016). Photodeoxygenation of dinaphthothiophene, benzophenanthrothiophene, and benzonaphthothiophene: S-oxides. *Photochemical and Photobiological Sciences*, 15(6), 791–800. https://doi.org/10.1039/c5pp00466g
- Chintala, S. M., Petroff, J. T., Barnes, A., & McCulla, R. D. (2019). Photodeoxygenation of phenanthro[4,5-bcd]thiophene S-oxide, triphenyleno[1,12-bcd]thiophene S-oxide and perylo[1,12-bcd]thiophene S-oxide. *Journal of Sulfur Chemistry*, 40(5), 503–515. https://doi.org/10.1080/17415993.2019.1615065
- 11. Korang, J., Grither, W. R., & McCulla, R. D. (2010). Photodeoxygenation of dibenzothiophene S-oxide derivatives in aqueous

- media. Journal of the American Chemical Society, 132(12), 4466–4476. https://doi.org/10.1021/ja100147b
- Omlid, S., Isor, A., Sulkowski, K., Chintala, S., Petroff, J., & McCulla, R. (2018). Synthesis of aromatic disulfonic acids for water-soluble dibenzothiophene derivatives. *Synthesis*, 50(12), 2359–2366. https://doi.org/10.1055/s-0036-1591969
- Isor, A., Chartier, B. V., Abo, M., Currens, E. R., Weerapana, E., & McCulla, R. D. (2021). Identifying cysteine residues susceptible to oxidation by photoactivatable atomic oxygen precursors using a proteome-wide analysis. RSC Chemical Biology, 2(2), 577–591. https://doi.org/10.1039/d0cb00200c
- Zhang, M., Ravilious, G. E., Hicks, L. M., Jez, J. M., & McCulla, R. D. (2012). Redox switching of adenosine-5'-phosphosulfate kinase with photoactivatable atomic oxygen precursors. *Journal of the American Chemical Society*, 134(41), 16979–16982. https://doi.org/10.1021/ja3078522
- Korang, J., Emahi, I., Grither, W. R., Baumann, S. M., Baum, D. A., & McCulla, R. D. (2013). Photoinduced DNA cleavage by atomic oxygen precursors in aqueous solutions. *RSC Advances*, 3(30), 12390–12397. https://doi.org/10.1039/c3ra41597j
- Bourdillon, M. T., Ford, B. A., Knulty, A. T., Gray, C. N., Zhang, M., Ford, D. A., & McCulla, R. D. (2014). Oxidation of plasmalogen, low-density lipoprotein and raw 264.7 cells by photoactivatable atomic oxygen precursors. *Photochemistry* and *Photobiology*, 90(2), 386–393. https://doi.org/10.1111/php. 12201
- Petroff, J. T., Isor, A., Chintala, S. M., Albert, C. J., Franke, J. D., Weinstein, D., Omlid, S. M., Arnatt, C. K., Ford, D. A., & McCulla, R. D. (2020). In vitro oxidations of low-density lipoprotein and RAW 264.7 cells with lipophilic O(3P)-precursors. RSC Advances, 10(44), 26553–26565. https://doi.org/10.1039/D0RA0 1517B
- Patrick, G. L. (2013). Prodrugs to improve membrane permeability. An introduction to medicinal chemistry (5th ed., p. 259).
 Oxford University Press.
- Kalyanaraman, B., Cheng, G., Hardy, M., Ouari, O., Bennett, B., & Zielonka, J. (2018). Teaching the basics of reactive oxygen species and their relevance to cancer biology: Mitochondrial reactive oxygen species detection, redox signaling, and targeted therapies. *Redox Biology*, 15, 347–362. https://doi.org/10.1016/j.redox.2017. 12.012
- Fleury, C., Mignotte, B., & Vayssière, J. L. (2002). Mitochondrial reactive oxygen species in cell death signaling. *Biochimie*, 84(2– 3), 131–141. https://doi.org/10.1016/S0300-9084(02)01369-X
- Redza-Dutordoir, M., & Averill-Bates, D. A. (2016). Activation of apoptosis signalling pathways by reactive oxygen species. *Biochimica et Biophysica Acta*, 1863(12), 2977–2992. https://doi.org/ 10.1016/j.bbamcr.2016.09.012
- Circu, M. L., & Aw, T. Y. (2010). Reactive oxygen species, cellular redox systems, and apoptosis. Free Radical Biology and Medicine, 48(6), 749–762. https://doi.org/10.1016/j.freeradbiomed.2009.12.022
- Petroff, J. T., Skubic, K. N., Arnatt, C. K., & McCulla, R. D. (2018). Asymmetric dibenzothiophene sulfones as fluorescent nuclear stains. *Journal of Organic Chemistry*, 83(22), 14063–14068. https://doi.org/10.1021/acs.joc.8b01931
- Petroff, J. T., Grady, S., Arnatt, C. K., & McCulla, R. D. (2020). Dibenzothiophene sulfone derivatives as plasma membrane dyes. *Photochemistry and Photobiology*, 96(1), 67–73. https://doi.org/10.1111/php.13175
- Isor, A., O'Dea, A. T., Petroff, J. T., Skubic, K. N., Grady, S. F., Arnatt, C. K., & McCulla, R. D. (2020). Synthesis of triphenylphosphonium dibenzothiophene S-oxide derivatives and their effect on cell cycle as photodeoxygenation-based cytotoxic agents. *Bioorganic Chemistry*, 105(2020), 104442–104454. https://doi.org/10.1016/j.bioorg.2020.104442



- Schindelin, J., Arganda-Carreras, I., Frise, E., Kaynig, V., Longair, M., Pietzsch, T., Preibisch, S., Rueden, C., Saalfeld, S., Schmid, B., Tinevez, J. Y., White, D. J., Hartenstein, V., Eliceiri, K., Tomancak, P., & Cardona, A. (2012). Fiji: An open-source platform for biological-image analysis. *Nature Methods*, 9(7), 676–682. https://doi.org/10.1038/nmeth.2019
- Callegari, A. J., & Kelly, T. J. (2007). Shedding light on the DNA damage checkpoint. *Cell Cycle*, 6(6), 660–666. https://doi.org/10.4161/cc.6.6.3984
- 28. R Core Team. (2020). R: A language and environment for statistical computing. R Foundation for Statistical Computing, Vienna, Austria URL http://www.R-projectorg/
- Kolde, R. (2015). Pheatmap: Pretty Heatmaps. R package version 1.0.12. http://cran.r-project.org/web/packages/pheatmap/index. html
- Online Mendelian Inheritance in Man, OMIM. (2021). McKusick–Nathans Institute of Genetic Medicine, Johns Hopkins University (Baltimore, MD) and National Center for Biotechnology Information, National Library of Medicine (Bethesda, MD). https://omim.org/.
- Png, K. J., Halberg, N., Yoshida, M., & Tavazoie, S. F. (2012).
 A microRNA regulon that mediates endothelial recruitment and metastasis by cancer cells. *Nature*, 481(7380), 190–194. https://doi.org/10.1038/nature10661
- 32. Polesskaya, A., Cuvellier, S., Naguibneva, I., Duquet, A., Moss, E. G., & Harel-Bellan, A. (2007). Lin-28 binds IGF-2 mRNA and participates in skeletal myogenesis by increasing translation efficiency. *Genes and Development*, 21(9), 1125–1138. https://doi.org/10.1101/gad.415007
- Yu, J., Vodyanik, M. A., Smuga-Otto, K., Antosiewicz-Bourget, J., Frane, J. L., Tian, S., Nie, J., Jonsdottir, G. A., Ruotti, V., Stewart, R., Slukvin, I. I., & Thomson, J. A. (2007). Induced pluripotent stem cell lines derived from human somatic cells. *Science*, 318(5858), 1917–1920. https://doi.org/10.1126/science.1151526
- Takefuji, M., Asano, H., Mori, K., Amano, M., Kato, K., Watanabe, T., Morita, Y., Katsumi, A., Itoh, T., Takenawa, T., Hirashiki, A., Izawa, H., Nagata, K., Hirayama, H., Takatsu, F., Naoe, T., Yokota, M., & Kaibuchi, K. (2010). Mutation of ARHGAP9 in patients with coronary spastic angina. *Journal of Human Genetics*, 55(1), 42–49. https://doi.org/10.1038/jhg.2009.120
- Furukawa, Y., Kawasoe, T., Daigo, Y., Nishiwaki, T., Ishiguro, H., Takahashi, M., Kitayama, J., & Nakamura, Y. (2001). Isolation of a novel human gene, ARHGAP9, encoding a Rho-GTPase activating protein. *Biochemical and Biophysical Research Communica*tions, 284(3), 643–649. https://doi.org/10.1006/bbrc.2001.5022
- 36. Blighe, K., Rana, S., & Lewis, M. (2020). Enhanced volcano: Publication-ready volcano plots with enhanced colouring and labeling. version 1.12.0. https://github.com/kevinblighe/EnhancedVolcano.
- Gentleman, R. C., Carey, V. J., Bates, D. M., Bolstad, B., Dettling, M., Dudoit, S., Ellis, B., Gautier, L., Ge, Y., Gentry, J., Hornik, K., Hothorn, T., Huber, W., Iacus, S., Irizarry, R., Leisch, F., Li, C., Maechler, M., Rossini, A. J., ... Zhang, J. (2004). Bioconductor: Open software development for computational biology and bioinformatics. *Genome Biology*, 5(10), R80. https://doi.org/10.1186/gb-2004-5-10-r80
- Chen, J., Bardes, E. E., Aronow, B. J., & Jegga, A. G. (2009). ToppGene Suite for gene list enrichment analysis and candidate gene prioritization. *Nucleic Acids Research*, 37, W305–W311. https://doi.org/10.1093/nar/gkp427
- Chen, J., Aronow, B. J., & Jegga, A. G. (2009). Disease candidate gene identification and prioritization using protein interaction networks. *BMC Bioinformatics*, 10(1), 73. https://doi.org/10.1186/ 1471-2105-10-73
- 40. Chen, J., Xu, H., Aronow, B. J., & Jegga, A. G. (2007). Improved human disease candidate gene prioritization using mouse

- phenotype. *BMC Bioinformatics*, 8(1), 392. https://doi.org/10. 1186/1471-2105-8-392
- 41 Lyall, R., Nikoloski, Z., & Gechev, T. (2020). Comparative analysis of ROS network genes in extremophile eukaryotes. *International Journal of Molecular Sciences*. https://doi.org/ 10.3390/ijms21239131
- Carbon, S., Ireland, A., Mungall, C. J., Shu, S., Marshall, B., & Lewis, S. (2009). AmiGO: Online access to ontology and annotation data. *Bioinformatics*, 25(2), 288–289. https://doi.org/ 10.1093/bioinformatics/btn615
- 43. Riss, T. L., Moravec, R. A., Niles, A. L., Duellman, S., Benink, H. A., Worzella, T. J., & Minor, L., et al. (2004). Cell viability assays. In S. Markossian, A. Grossman, & K. Brimacombe (Eds.), Assay guidance manual. Eli Lilly and Company and the National Center for Advancing Translational Sciences.
- Edgar, R. (2002). Gene expression omnibus: NCBI gene expression and hybridization array data repository. *Nucleic Acids Research*, 30(1), 207–210. https://doi.org/10.1093/nar/30.1.207
- Barrett, T., Wilhite, S. E., Ledoux, P., Evangelista, C., Kim, I. F., Tomashevsky, M., Marshall, K. A., Phillippy, K. H., Sherman, P. M., Holko, M., Yefanov, A., Lee, H., Zhang, N., Robertson, C. L., Serova, N., Davis, S., & Soboleva, A. (2013). NCBI GEO: Archive for functional genomics data sets-Update. *Nucleic Acids Research*, 41, D991–D995. https://doi.org/10.1093/nar/gks1193
- Huber, W., Carey, V. J., Gentleman, R., Anders, S., Carlson, M., Carvalho, B. S., Bravo, H. C., Davis, S., Gatto, L., Girke, T., Gottardo, R., Hahne, F., Hansen, K. D., Irizarry, R. A., Lawrence, M., Love, M. I., MacDonald, J., Obenchain, V., Oles, A. K., ... Morgan, M. (2015). Orchestrating high-throughput genomic analysis with Bioconductor. *Nature Methods*, 12(2), 115–121. https://doi. org/10.1038/nmeth.3252
- Kanehisa, M., & Goto, S. (2000). KEGG: Kyoto encyclopedia of genes and genomes. *Nucleic Acids Research*, 28(1), 27–30. https:// doi.org/10.1093/nar/28.1.27
- Kanehisa, M. (2019). Toward understanding the origin and evolution of cellular organisms. *Protein Science*, 28(11), 1947–1951. https://doi.org/10.1002/pro.3715
- Kanehisa, M., Furumichi, M., Sato, Y., Ishiguro-Watanabe, M., & Tanabe, M. (2021). KEGG: Integrating viruses and cellular organisms. *Nucleic Acids Research*, 49(D1), D545–D551. https:// doi.org/10.1093/nar/gkaa970
- Nishimura, D. (2001). BioCarta. Biotech Software and Internet Report, 2(3), 117–120. https://doi.org/10.1089/152791601750294 344
- Karp, P. D., Billington, R., Caspi, R., Fulcher, C. A., Latendresse, M., Kothari, A., Keseler, I. M., Krummenacker, M., Midford, P. E., Ong, Q., Ong, W. K., Paley, S. M., & Subhraveti, P. (2019). The BioCyc collection of microbial genomes and metabolic pathways. *Briefings in Bioinformatics*, 20(4), 1085–1093. https://doi. org/10.1093/bib/bbx085
- Fabregat, A., Korninger, F., Viteri, G., Sidiropoulos, K., Marin-Garcia, P., Ping, P., Wu, G., Stein, L., D'Eustachio, P., & Hermjakob, H. (2018). Reactome graph database: Efficient access to complex pathway data. *PLoS Computational Biology*, 14(1), e1005968. https://doi.org/10.1371/journal.pcbi.1005968
- Fabregat, A., Sidiropoulos, K., Viteri, G., Forner, O., Marin-Garcia, P., Arnau, V., D'Eustachio, P., Stein, L., & Hermjakob, H. (2017). Reactome pathway analysis: A high-performance inmemory approach. *BMC Bioinformatics*, 18(1), 142. https://doi.org/10.1186/s12859-017-1559-2
- Fabregat, A., Sidiropoulos, K., Viteri, G., Marin-Garcia, P., Ping, P., Stein, L., D'Eustachio, P., & Hermjakob, H. (2018). Reactome diagram viewer: Data structures and strategies to boost performance. *Bioinformatics*, 34(7), 1208–1214. https://doi.org/10. 1093/bioinformatics/btx752



- 55. Jassal, B., Matthews, L., Viteri, G., Gong, C., Lorente, P., Fabregat, A., Sidiropoulos, K., Cook, J., Gillespie, M., Haw, R., Loney, F., May, B., Milacic, M., Rothfels, K., Sevilla, C., Shamovsky, V., Shorser, S., Varusai, T., Weiser, J., ... D'Eustachio, P. (2020). The reactome pathway knowledgebase. *Nucleic Acids Research*, 48(D1), D498–D503. https://doi.org/10.1093/nar/gkz1031
- Sidiropoulos, K., Viteri, G., Sevilla, C., Jupe, S., Webber, M., Orlic-Milacic, M., Jassal, B., May, B., Shamovsky, V., Duenas, C., Rothfels, K., Matthews, L., Song, H., Stein, L., Haw, R., D'Eustachio, P., Ping, P., Hermjakob, H., & Fabregat, A. (2017). Reactome enhanced pathway visualization. *Bioinformatics*, 33(21), 3461–3467. https://doi.org/10.1093/bioinformatics/btx441
- Wu, G., & Haw, R. (2017). Functional interaction network construction and analysis for disease discovery. *Methods in Molecular Biology*, 1558, 235–253. https://doi.org/10.1007/978-1-4939-6783-4
- Dahlquist, K. D., Salomonis, N., Vranizan, K., Lawlor, S. C., & Conklin, B. R. (2002). GenMAPP, a new tool for viewing and analyzing microarray data on biological pathways. *Nature Genetics*, 31(1), 19–20. https://doi.org/10.1038/ng0502-19

- Liberzon, A., Birger, C., Thorvaldsdottir, H., Ghandi, M., Mesirov, J. P., & Tamayo, P. (2015). The molecular signatures database (MSigDB) hallmark gene set collection. *Cell Systems*, 1(6), 417–425. https://doi.org/10.1016/j.cels.2015.12.004
- 60 Liberzon, A., Subramanian, A., Pinchback, R., Thorvaldsdottir, H., Tamayo, P., & Mesirov, J. P. (2011). Molecular signatures database (MSigDB) 3.0. *Bioinformatics*, 27(12), 1739–1740. https://doi.org/10.1093/bioinformatics/btr260
- Subramanian, A., Tamayo, P., Mootha, V. K., Mukherjee, S., Ebert, B. L., Gillette, M. A., Paulovich, A., Pomeroy, S. L., Golub, T. R., Lander, E. S., & Mesirov, J. P. (2005). Gene set enrichment analysis: A knowledge-based approach for interpreting genomewide expression profiles. *Proceedings of the National Academy* of Sciences, 102(43), 15545–15550. https://doi.org/10.1073/pnas. 0506580102
- 62 Petri, V., Shimoyama, M., Hayman, G. T., Smith, J. R., Tutaj, M., de Pons, J., et al. (2011). The rat genome database pathway portal. *Database*. https://doi.org/10.1093/database/bar010Suns.

